Heating load reduction strategies for cabin and battery climatization in electric trucks operating in cold climates

(article starts on next page)

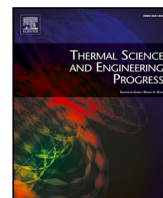# Heating load reduction strategies for cabin and battery climatization in electric trucks operating in cold climates☆

Anandh Ramesh Babu [a], Simone Sebben [a,*], Zenitha Chronéer [b], Sassan Etemad [a,b]

[a] *Chalmers University of Technology, Gothenburg, Sweden*
[b] *Volvo Group Truck Technology, Gothenburg, Sweden*

A B S T R A C T

To improve the efficiency of energy usage in battery electric vehicles, effective thermal management strategies are crucial, particularly in cold climates, because of higher energy consumption due to increased auxiliary energy demand for cabin and battery climatization. In this paper, the influence of auxiliary heating load reduction strategies on vehicle performance was numerically investigated for an electric truck operating in parking-driving scenarios at various ambient temperatures. The load reduction strategies included cabin insulation, cabin air recirculation, and thermal encapsulation of the battery pack. The results showed that for the baseline vehicle, auxiliary energy consumption increased more than fivefold when ambient temperature was reduced from 10°C to −20°C. When all strategies were used, the heating loads for both the cabin and the battery decreased, leading to an increase in the vehicle range at low ambient temperatures up to 7% at −20°C. At high relative humidity, or with more occupants, the degree of cabin air recirculation that could be employed was reduced, resulting in lower range gains.

1. Introduction

The transition to battery electric vehicles (BEVs) marks a significant shift in the automotive industry and brings forth unique challenges to the vehicle thermal management systems (VTMS). The VTMS is a crucial subsystem that ensures a comfortable cabin for the occupants and that the components, particularly the battery pack and the motors are climatized to the appropriate temperatures for optimal energy utilization, extending their lifetimes. The choice of VTMS strategies employed has a strong influence on the energy consumption of BEVs.

A parameter known to largely affect the driving range of BEVs is the ambient temperature, particularly at conditions below 10°C. Several real-world tests have been conducted to investigate the influence of the ambient temperature on the energy consumption. These studies have been consistent in reporting increasing energy consumption with decreasing ambient temperatures. The reasons for the poor low-temperature performance are high rolling and aerodynamic resistances [1,2], high auxiliary loads, and poor battery performance [1,3–5].

The heating ventilation and air conditioning (HVAC) system is one of the largest auxiliary loads in the vehicle which ensures safe driving by defogging and defrosting the windows and provides thermal comfort

for the occupants [6]. At low temperatures the HVAC load increases, consequently causing a reduction in driving range. Zhang et al. [7] showed that the ventilation load during heating was more than 70% of the total HVAC load, while the rest was due to the ambient load, which tends to increase with decreasing ambient temperatures. The high heating load while using a positive thermal coefficient (PTC) heater caused a range reduction of up to 54%. Yuksel and Michalek [4] reported a 65% increase in energy consumption at −30°C, while Taggart [1] showed a 40% increase at −10°C as compared to that at 20°C ambient temperature. Steinstraeter et al. [5] found a range decrease of about 50% due to heating demand and limited battery recuperation. About 32% of the net energy for the trip was spent on cabin heating and about 22% was lost due to limited battery recuperation.

Regarding battery performance, lithium-ion batteries (LIBs) at low operating temperatures, have noted decreased energy and power capabilities [8]. Several studies have investigated LIBs at low temperatures, and have put forth many effects influencing their performance such as increased resistance due to low electrolyte conductivity, slow kinetics, polarization of the anode leading to lithium plating resulting in capacity loss and so on [9–11]. Additionally, fast charging at low cell temperatures and at high state of charge (SoC) should be avoided

Nomenclature

Abbreviations

0D	Zero dimensional
BEV	Battery electric vehicle
BMS	Battery management system
CFD	Computational fluid dynamics
ECM	Electrical circuit model
HVAC	Heating ventilation and air conditioning
LIB	Lithium-ion battery
NMC	Nickel Manganese Cobalt
OSA	Outside air
PI	Proportional integral
PTC	Positive thermal coefficient
RAR	Return-air ratio
RC	Resistance capacitance
REC	Recirculated air
RH	Relative humidity
RMSE	Root mean squared error
SoC	State of charge
TXV	Expansion valve
VTMS	Vehicle thermal management system

Symbols

P_v	Traction power
M_v	Vehicle mass
a_v	Vehicle acceleration
ρ	Air density
v_v	Vehicle velocity
C_d	Drag coefficient
A_{f_v}	Frontal area of the vehicle
μ_r	Rolling resistance coefficient
g	Acceleration due to gravity
β	Road gradient
T	Temperature
θ	Non-dimensional temperature
θ_{set}	Normalized setpoint margin
$T_{w,mean}$	Mean window temperature
$T_{target,dp}$	Target dew-point temperature
γ	Recirculation or return-air ratio
α	CO_2 concentration
ω	Specific humidity
t	Time
τ	Thermal time constant
R_{th}	Thermal resistance
Y	Road curvature
v_{legal}	Road legal speed
Q_{amb}	Heat loss to the ambient
c_p	Specific heat
T_{bo}	Temperature upstream of the heater

Subscripts

0	Initial condition
set	Set-point for the corresponding quantity
cab	Mean quantity in the cabin
∞	Ambient condition
bo	Upstream condition to the heater
in	Inlet condition of a quantity
ω	Humidity-critical condition
α	CO_2-critical condition
h	Source

to prevent lithium plating [12]. To prevent battery life deterioration, many battery manufacturers disable/limit charging at subzero temperatures in the battery management system (BMS) [3,5]. Furthermore, the cells are heated using coolant heaters to optimal operating temperatures for improved longevity [13]. However, this increases the auxiliary demand leading to decreased driving range.

To reduce the impact of the heating loads, methods of efficient heat delivery, and of heating load reduction have been investigated. The former typically employs waste-heat recovery strategies, and heat pumps [14–16] to deliver the required heat efficiently. Such solutions are more common in passenger vehicles but their architecture is still under development for commercial vehicles. The latter methods aim at reducing the heating loads using thermal insulation, phase change materials, localized climatization, and cabin air recirculation [16–20].

In the previous works by the authors, three heating load reduction strategies were investigated. Using computational fluid dynamics (CFD) simulations, the use of cabin insulation to reduce the ambient load while driving was investigated under a constant HVAC heating load [21]. A conjugate heat transfer model of a cabin was developed and thermally insulating material was fastened to the cabin solids to reduce heat loss from the cabin air to solid, resulting in higher cabin temperatures. The use of adaptive recirculation to reduce the cabin ventilation load was investigated using a similar CFD approach, with a coupled thermoregulation model to account for heat, vapor, and CO_2 sources from an occupant in the cabin [22]. The heating was controlled using a PI controller to avoid fogging and to maintain air quality, and this method reduced the heating load by up to 34% as compared to a case without recirculation. Considering that in modern electric trucks, cabin recirculation is not a standard practice for ambient temperatures below 20°C to prevent windshield fogging, this strategy is very promising. Additionally, battery pack thermal encapsulation was studied as a means of passive battery thermal management to reduce heat loss during periods of cooldown [23]. It was found that the thermal resistance of the encapsulating material is the key parameter that determines the temperature decay.

While the aforementioned studies have shown that these strategies are beneficial to reduce the heating energy consumption at the component level, their effects on the energy consumption and driving range at the vehicle level still need to be evaluated. Moreover, with the advent of electric trucks, more investigations are necessary to assess the effectiveness of each strategy. In this work, an effort towards understanding the effects of employing these heating load reduction strategies holistically, at the vehicle level, is taken. An electric truck is systematically modeled with various subsystems, along with validated battery pack and cabin models. First, the influence of ambient temperature on the driving range is studied for five ambient temperatures ranging from −20°C to 20°C, followed by the effects of heating load reduction strategies on the auxiliary energy consumption and vehicle performance. Finally, the influence of ambient relative humidity (RH) and number of occupants are discussed.

2. Methodology

2.1. Vehicle subsystems

The vehicle considered was a fully electric truck and its main specifications are presented in Table 1. Fig. 1 illustrates a schematic of the truck model. Three main vehicle subsystems were considered: a simplified vehicle powertrain model, the vehicle thermal management system, and the system controllers.

2.1.1. Vehicle powertrain

The vehicle had three axles, each assumed to be equally weighted and were driven by an electric motor through a differential. The electric motors also served as generators to regenerate energy while braking. The efficiency map of the electric machine as a function of the normalized torque and speed is shown in Fig. 2. According to Newton's law, the traction power was calculated as (see [24])

$$P_v = \left(M_v a_v + \frac{1}{2}\rho v_v^2 C_d A_{f_v} + \mu_r M_v g\cos(\beta) + M_v g\sin(\beta) \right) v_v \tag{1}$$
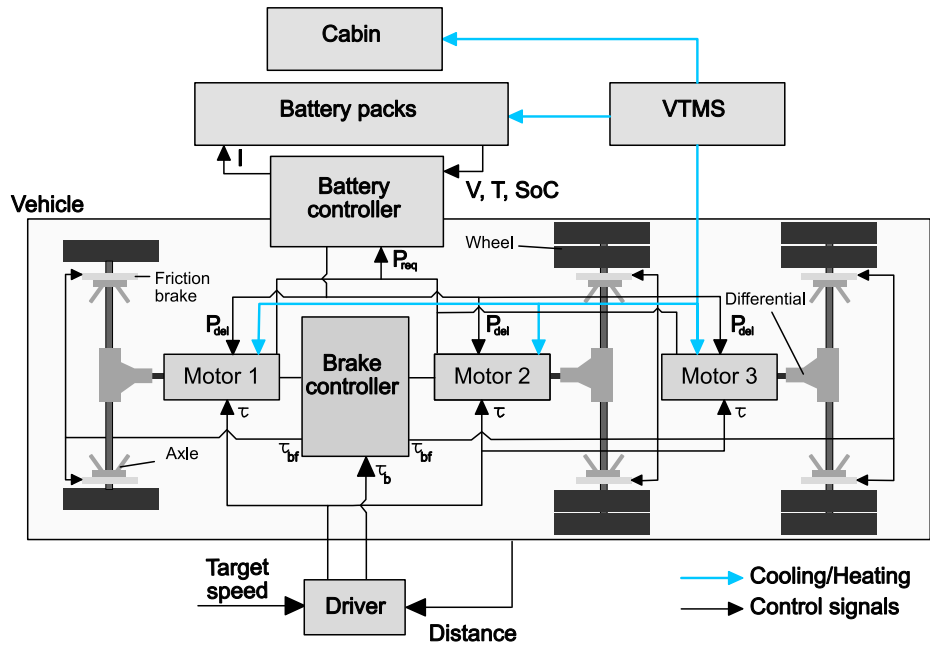
Fig. 1. Schematic of the simplified truck model with three main subsystems: powertrain model, thermal management system and controllers.

Table 1
Truck specifications.

Parameter	Value
Vehicle mass (M_v)	20 000 kg
Drag coefficient (C_d)	0.5
Frontal area (A_{f_v})	10 m²
Gear-train efficiency	0.855

where M_v is the mass of the vehicle, a_v is the acceleration, ρ is the density of air, v_v is the velocity of the vehicle, C_d is the coefficient of drag, A_{f_v} is the frontal area, μ_r is the rolling resistance coefficient of the tyre, g is the acceleration due to gravity and β is the road gradient. In this study, only a flat road was considered and hence, β was zero.

To account for the variation in the traction load due to operating temperatures, the air density was modeled based on the ideal gas equation accounting for ambient temperature at 1 bar pressure. The drag coefficient C_d was considered to have a constant value of 0.5 (assuming zero yaw and no wind), though it can show slight variations at different operating temperatures. The rolling resistance coefficient was modeled based on the works of Hyttenin [2] where it was defined as a function of the tyre temperature and vehicle velocity. The tyre temperature was initialized to the same as the ambient, and its variation was computed based on the ambient temperature and vehicle velocity. The rolling resistance coefficient was then computed instantaneously as a function of velocity and tyre temperature.

The electric machines received information about the maximum discharge/charge ability (discussed below in Section 2.1.3) of the batteries during each timestep in the simulation. During braking, the brake controller unit received messages about the maximum charging power of the batteries and the maximum braking torque of the motors. If the regenerated power was lower than the maximum charge threshold, the batteries were charged whereas if the regenerated power exceeded the maximum threshold, the batteries charged at their limits, and the friction brakes supplied the rest of the braking torque. The electrical losses to/from the battery pack were assumed to be 8%. Finally, the vehicle was driven by a driver model whose input was a prescribed target speed (discussed in Section 4). The driver model requested torque equally from the three electric motors to match the vehicle speed and the target speed.
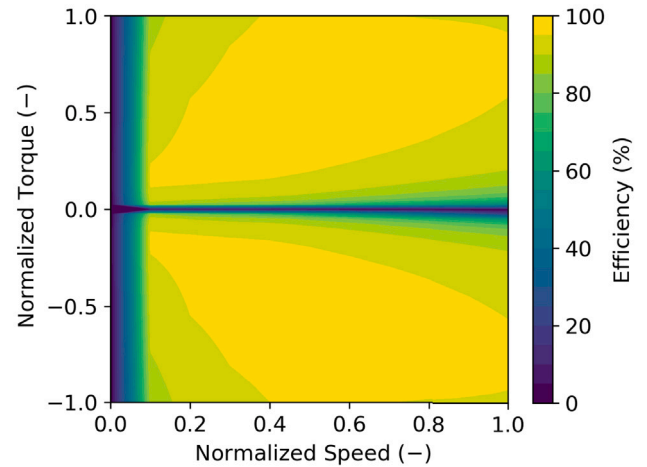

Fig. 2. Electric machine efficiency map as a function of normalized torque and speed. The quantities have been normalized with respect to their corresponding maximum operating values.

2.1.2. Vehicle thermal management system

The thermal management architecture for the vehicle consisted of five circuits, as shown in the schematic in Fig. 3.

- The vehicle included six battery packs and coolant hoses were connected in parallel to each pack. The battery circuit had a pump and heater in series, and a chiller for cooling using the refrigerant loop. The chiller was operated when the battery pack temperature was above 28°C, and until the pack temperature decreased below 26°C. The 10 kW heater downstream of the pump was employed for battery heating if the initial average temperature of the battery pack was below 15°C. The battery circuit was opened to the E-machines circuit using valve V2 if battery pack heating was necessary and when the temperature in the outer loop was suitable for heating.

- The components in the E-machines circuit were connected in series, while identical components, i.e., each of the three motors,
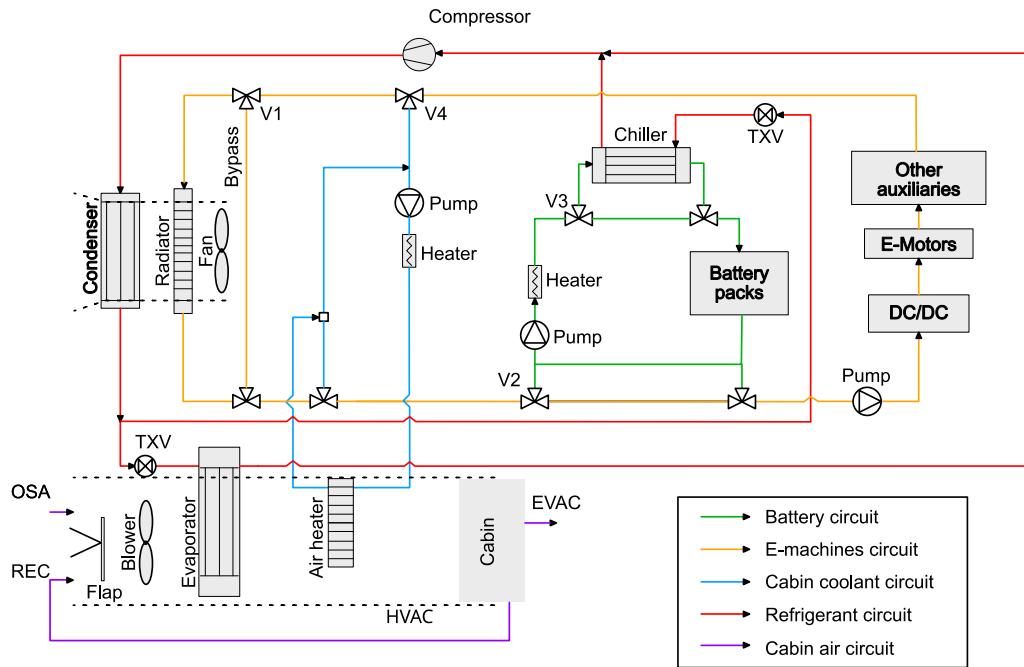
Fig. 3. Schematic of the vehicle thermal management system and its five circuits.

were connected in parallel with the others. The E-machines circuit included a radiator for cooling. A thermostat was modeled to regulate the temperature in the circuit by allowing coolant to bypass the radiator when necessary, using valve V1.

- The cabin coolant circuit consisted of three components: a pump, a coolant-heater, and an air-heater to heat the cabin air entering the cabin. The waste heat from the E-machines circuit was used for this purpose if the temperature was between 1°C and 3°C above the required temperature of the coolant using valve V4. Outside this operating condition, the heater was employed to achieve the required inlet air temperature.

- The refrigerant circuit was modeled for dehumidifying the cabin air at the evaporator, along with a secondary loop equipped with a chiller for battery cooling. A variable-speed compressor was used, and the speed was regulated based on the cooling request at the chiller and evaporator. To achieve the desired effect at the heat exchangers, the coolant flow rate at the chiller was regulated with valve V3 controlled by a PI controller. Expansion valves (TXV) upstream of the evaporator and chiller were employed to expand the hot refrigerant. They were operated to achieve a target degree of superheat upstream of the compressor. The evaporator was operated when the dew point temperature of the ambient air was above 5°C, aiming to cool down the air to 3°C. The chiller operated if the average battery pack temperature was above 28°C, and cooled until the average temperature was below 26°C.

- The cabin air circuit was used to climatize the cabin. The main components of this circuit are a blower, an evaporator, an air-heater, and cabin. The blower drew air from the ambient outside air (OSA) and/or the cabin through recirculation (REC). The blower speed was set depending on the ambient temperature and maintained throughout the simulation. The temperature in the cabin air circuit was controlled by the evaporator and the cabin air-heater, aiming to maintain 22°C. The cabin coolant heater rate was limited such that the maximum air temperature entering the cabin during heating was $40-T_{\infty}$ (°C) [22]. The requested recirculation ratio was achieved through a PI-controlled flap as shown in the figure. PI-controllers are very common in the automotive industry as they are cheap, and easy to implement.

A fan was placed in the under-hood compartment downstream of the radiator and was used when the vehicle velocity was less than 10 km/h, and if there was either coolant flow through the radiator or refrigerant flow through the condenser. Finally, a deaeration system (not shown in Fig. 3) was included to prevent overpressure due to coolant expansion under heating or to supplement the primary systems with additional coolant when coolant contracts under cooling, which would otherwise create a negative pressure. In addition, the expansion tank aids in preventing cavitation by providing a high pressure upstream of the pump. The power required to run the auxiliary components was considered during vehicle operation.

The battery pack modeling approach used was similar to that presented by the authors in [23,25]. The pack had Li-ion cells arranged in several stacks or trays. Each tray included battery modules, an aluminum cooling plate for the coolant to flow through, and a thermal interface material between the modules and the cooling plate. Each module had several prismatic NMC-type Li-ion cells. The battery pack model was discretized at the module level, i.e, the cells in each battery module were represented as a single thermal mass. This facilitated simulations at the vehicle level with a good trade-off between accuracy and computational resources. The consequence is that all cells in the module have identical states. A second-order (2RC) Thevenin electrical equivalent model (ECM) [26] was used to describe the electrical behavior of the battery cells along with Bernardi's thermal model [27] to account for heat generation.

The battery pack was calibrated using experimental data under cool-down and heat-up scenarios in a climate chamber. Fig. 4 presents a comparison between the non dimensional measured and simulated battery pack temperatures during a cool-down test under idle conditions. The ambient temperature was maintained at sub-zero temperatures for about 34 h and the average battery pack temperature was monitored. The results from the simulation agree with the measurements indicating that the heat loss from the battery pack to the ambient is captured very well. Excellent agreement was seen for the heat-up test, with a mean root-mean-squared error of less than 0.5°C, though not shown here. Battery pack thermal encapsulation was included as in [23] with plates of insulating material with a certain thickness and material properties attached to each side of the battery pack.
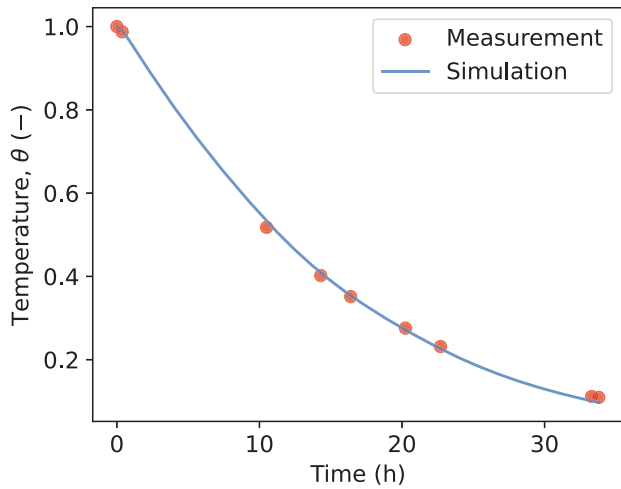
Fig. 4. Battery pack model calibration: comparison of measurements and simulation for the non-dimensional mean battery pack temperature during cool-down.
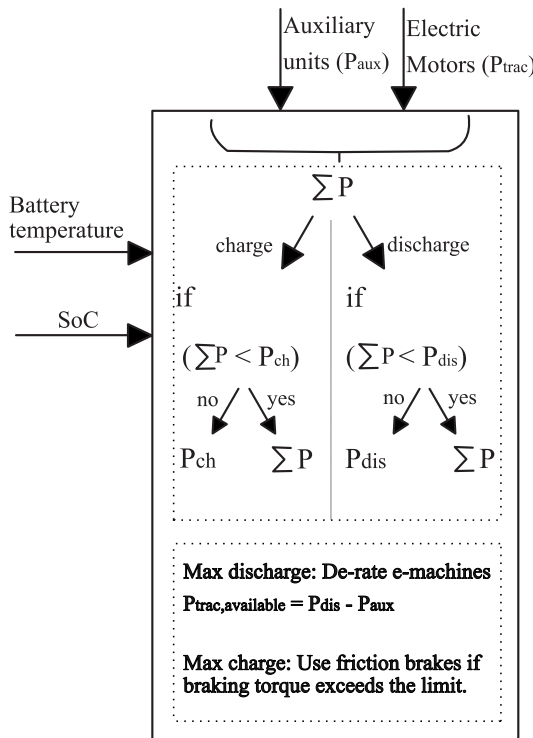

Fig. 5. Schematic of the vehicle battery management system.

The cabin air was modeled as a single control volume, where the transport equations for the temperature, CO_2, and humidity were solved in the time. The cabin solids were represented as lumped thermal masses, and heat transfer to these solids was calibrated by imposing suitable heat transfer coefficients to each solid as functions of HVAC inlet mass flow rate. The external heat transfer coefficient was imposed based on vehicle velocity as described in [22]. For the insulated cabin configuration, a thermal insulation material was included between the cabin air and the cabin solids to replicate the effects in [21].

2.1.3. System controllers

Battery management system

The simplified control logic for the battery pack simulations is shown in Fig. 5. The total electrical power, i.e., the sum of trac-
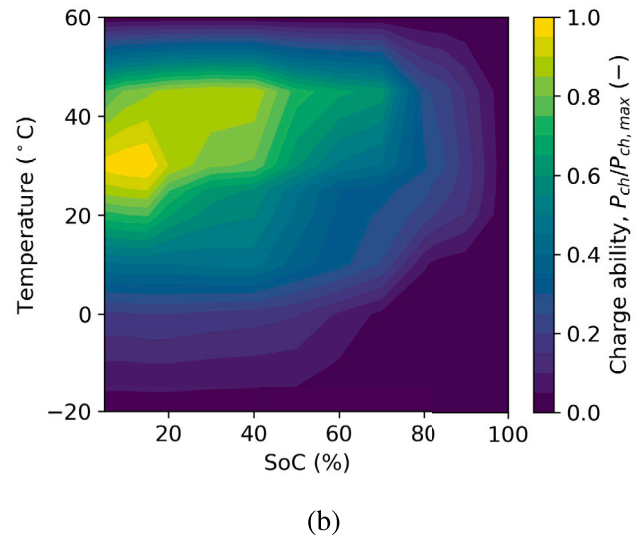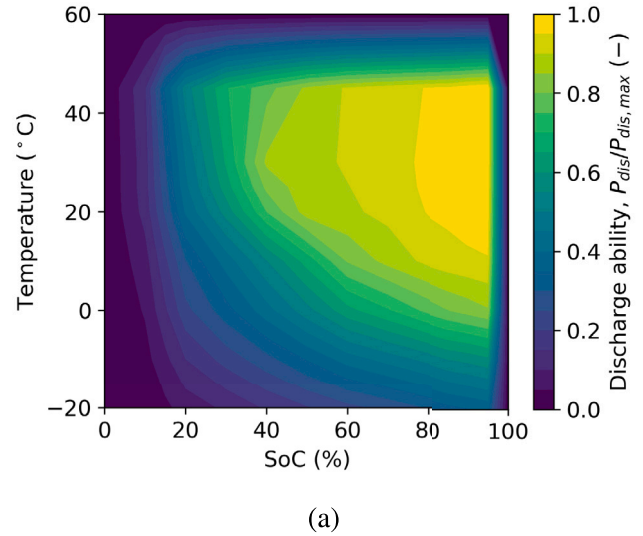

(a)

(b)

Fig. 6. Battery pack performance abilities as functions of SoC and temperature (a) Normalized battery discharge ability; (b) Normalized battery charge ability.

tion and auxiliary loads, requested/delivered from/to the pack was passed through the controller. This power was then converted to discharge/charge current from/to the battery pack based on its terminal voltage. Additionally, the battery pack's maximum discharge/charge ability in terms of power was considered in the controller for battery longevity. They were defined as functions of temperature and SoC as shown in Figs. 6(a) and 6(b). When the discharge power request from the batteries exceeded the limit, the E-machines were de-rated to accommodate the total auxiliary loads. If the power regenerated exceeded the charging ability, the batteries were charged at their limits, and friction brakes were employed for the rest of the braking torque.

Cabin air recirculation controller

In [22], CFD simulations were performed during cabin heating operation, and recirculation was controlled to target a dew-point temperature of 1°C below the minimum interfacial temperature between the cabin air and the windows. The simulations of the cabin at the vehicle level were performed with 0D models, with one control volume for air and lumped masses for the cabin solids and provided only the mean temperatures. Thus, the target dew-point ($T_{target,dp}$) must be reformulated with the mean window temperature ($T_{w,mean}$) with minimal window fogging. For this purpose, a normalized set-point
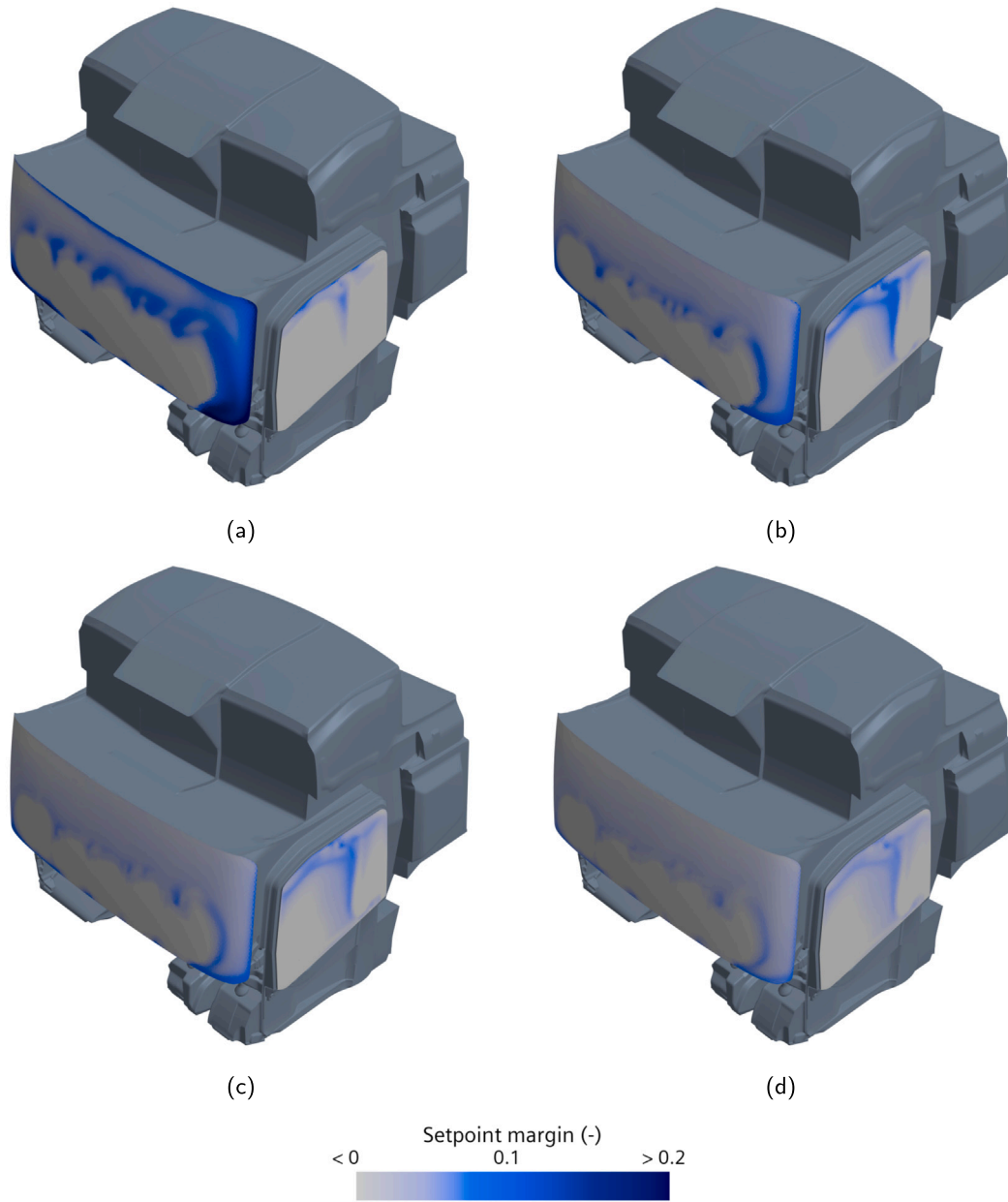
Fig. 7. Region of possible window fogging with varying normalized set-point margins according to 2 at driving speeds (a) 0 km/h; (b) 30 km/h; (c) 60 km/h; (d) 90 km/h.

margin (θ_{set}) was defined as,

$$\theta_{set} = \frac{T_{w,mean} - T_{target,dp}}{T_{in} - T_{\infty}} \tag{2}$$

where T_{in} is the inlet HVAC temperature into the cabin.

This quantity indicates the relative interval between the target dew-point and the mean window temperature for a given inlet and ambient temperature. The values for θ_{set} were determined based on steady-state CFD such that the 99.5% of the window area had interfacial temperatures greater than the $T_{target,dp}$. These computations were performed at selected driving speeds as shown in Fig. 7 and the values are tabulated in Table 2. To improve the robustness of the control strategy and energy savings, the target dew-point temperature had a lower bound of the ambient temperature, and was defined as,

$$T_{target,dp} = \max\left(T_{\infty}, T_{g,mean} - \theta_{set}(v_v) \cdot (T_{in} - T_{\infty})\right) \tag{3}$$

Table 2
Variation of normalized set-point margin at different driving speeds.

Driving speed (km/h)	Set-point margin (−)
0	0.19
30	0.105
60	0.081
90	0.066

Thus, the recirculation controller targeted a dew-point temperature based on the ambient temperature, the driving speed, and the mean windshield temperature.

The control strategy for the adaptive recirculation is defined based on the analytical solution for recirculation in a 0D cabin defined in [22] as,

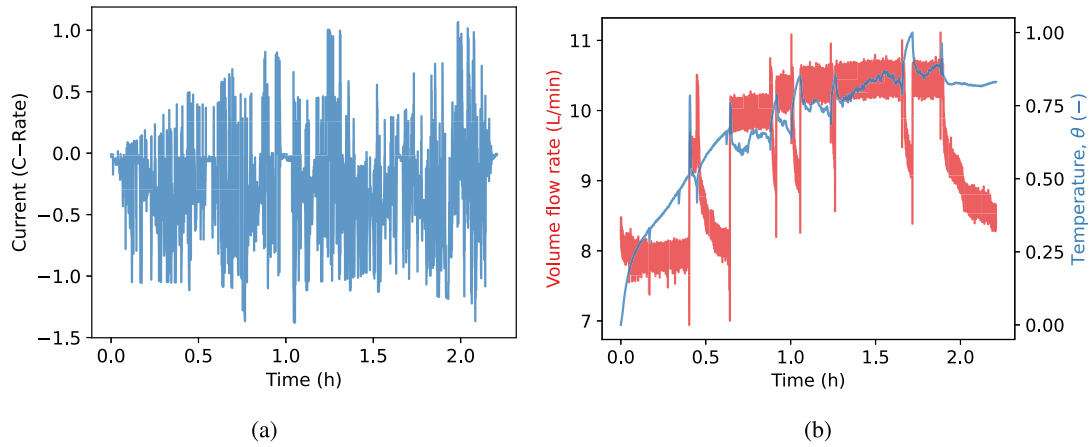$$\gamma = \min(\gamma_\alpha, \gamma_\omega) \tag{4}$$

Fig. 8. Battery pack validation scenario: (a) Requested current, and (b) Inlet volumetric flow rate and temperature of the coolant.

Table 3

RMSE and maximum errors between the measured and simulated quantities for the validation scenario.

Quantity	RMSE	Maximum error
Average pack temperature (°C)	0.633	1.308
Outlet coolant temperature (°C)	0.244	1.087
Normalized pack voltage (%)	1.34	6.5
SoC (%)	1.03	2.13

$$\gamma_\omega = \frac{1}{1 + \frac{\dot{m}_h \omega_h}{\dot{m}_{in}(\omega_{in,set} - \omega_\infty)}} \qquad (5)$$

$$\gamma_{\alpha,ss} = 1 - \frac{\dot{m}_h \alpha_h}{\dot{m}_{in}(\alpha_{set} - \alpha_\infty)} \qquad (6)$$

where γ is the recirculation ratio, α is CO_2 concentration, and ω is specific humidity, $\dot{m}_h \omega_h$ is the vapor source and assumed to be 42 g/h/occupant, $\dot{m}_h \alpha_h$ is the CO_2 source and assumed to be 21.6 g/h/occupant [28,29], $\dot{m}_{in}$ is the HVAC mass flow rate into the cabin, α_∞ is the ambient CO_2 at 420 ppm, α_{set} is the setpoint for CO_2 at 1000 ppm, ω_∞ is the specific humidity at ambient, and $\omega_{in,set}$ is the inlet specific humidity corresponding to the target dewpoint temperature in Eq. (3) at saturated conditions. Once the return-air ratio (RAR) was computed, the HVAC flap (in Fig. 3) was controlled with a PI controller such that the fresh and recirculated air into the cabin satisfied the target values.

2.2. Subsystem validation

The validations of the battery pack model using experimental data and the cabin model using a calibrated CFD procedure are presented below.

Battery pack model

Data measured from a truck during a winter expedition in Kiruna, Sweden, was used to validate the battery pack performance. Fig. 8(a) presents the requested current from the pack. The battery pack was initially cold, so the battery was heated using the heater during operation. The initial SoC of the battery pack was 83%, and the coolant flow rate and temperature into the battery pack are presented in Fig. 8(b).

Based on these inputs, four quantities namely, average battery pack temperature, coolant outlet temperature, terminal pack voltage, and SoC were evaluated as shown in Fig. 9. The root-mean-square errors (RMSE) and the maximum errors between the simulated and measured values are presented in Table 3. As seen, the trends and the results are in good agreement with the measurements.

Cabin model

In [22], a CFD model of the truck cabin was developed, and validated using test data from a climate chamber test. Using the CFD model, the 0D cabin model used in the vehicle simulations was calibrated and validated. Several steady-state computations were performed such that both the cabin models maintained identical volume averaged temperatures ($\approx$22°C), and the mean front window temperature, heat loss from cabin air to solids, and the heater energy required to maintain the required state were compared for a range of vehicle speeds at -10°C. Table 4 summaries the results of the validation study. The 0D cabin slightly over-predicted the results for all vehicle speeds as compared to the CFD cabin. The mean front window temperature was between 0.7°C and 1.35°C higher, while the heat losses and heater rates were under 0.1 kW and 0.2 kW, respectively. Based on these results, the 0D cabin model was considered to be sufficiently accurate for vehicle simulations. A validation of the 0D model with cabin insulation was also performed with good agreement.

3. Battery cool-down and thermal encapsulation characteristics

Cycles with long parking times between operation tend to cool-down the battery pack and require heating at restart. To reduce the required heating, an alternate approach is encapsulation of the battery pack to mitigate the heat loss. Since battery pack encapsulation is a fixed solution, it is important to choose the optimal insulation characteristics that best suit the truck operations. In [23], the authors investigated the effect of thermal encapsulation on the cool-down performance. Thermal resistance of the insulation material was identified as the key design parameter. In this section, a method to estimate the required encapsulation for a certain parking period such that battery heating is not required is explored.

In Fig. 10(a), cool-down trends are presented for the baseline and encapsulated battery packs with increasing thermal resistance. The battery pack was initialized to 23°C (T_0) at an ambient temperature of -20°C (T_∞). As the battery pack with encapsulation experiences reduced heat loss, the rate of cooling decreases with increasing thermal resistance, resulting in higher temperatures. Both the thermal conductivity and the encapsulation thickness of the insulating material were varied to achieve the respective resistance values. The results indicate that the temperature variation is an exponentially decaying process. This behavior can be captured [30] using equation,

$$\theta(t) = exp(-t/\tau) \qquad (7)$$

where τ is the thermal time constant, which represents the time it takes for the temperature to change by 63.2% of the temperature difference, and θ is the non-dimensional temperature.

$$\theta = \frac{T_b - T_\infty}{T_0 - T_\infty} \qquad (8)$$
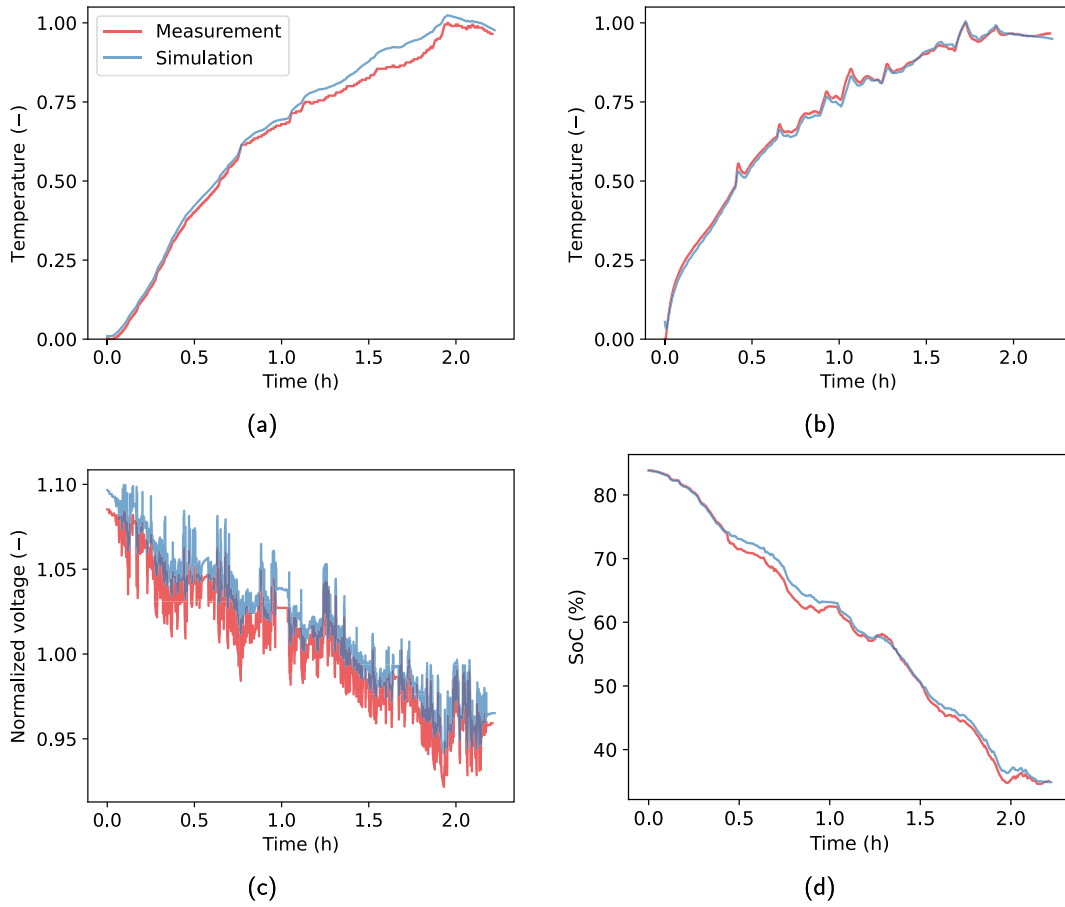
Fig. 9. Results for the validation scenario: (a) Normalized average battery pack temperature, (b) Normalized coolant outlet temperature, (c) Normalized terminal battery pack voltage, and (d) Battery pack SoC.

Table 4
Results for the cabin validation comparing CFD and 0D models at −10°C at selected driving speeds.

Vehicle speed (km/h)	Mean window temperature (°C)		Heat loss from air to solids (kW)		Heater rate (kW)	
	CFD cabin	0D cabin	CFD cabin	0D cabin	CFD cabin	0D cabin
0	7.25	8.6	0.77	0.85	3.87	4.07
30	−3.6	−2.3	1.1	1.13	4.15	4.32
60	−5.2	−4.5	1.16	1.19	4.21	4.39
90	−6.2	−5.5	1.19	1.22	4.25	4.45

The time constant for each simulated configuration was estimated, and is plotted in Fig. 10(b) as a function of the thermal resistance of encapsulation. The temperature decay that is obtained from Eq. (7) was within 1.5% of the simulated values for all cases. The thermal resistance of 0 m^2 K/W in the figure represents the baseline battery pack. With increasing thermal resistance, the time constant increases, i.e., the cooling process is delayed. Based on these results, a curve-fit was generated between thermal resistance and time constant,

$$\tau^*(R_{th}) = \frac{501 \cdot R_{th}^{0.867}}{R_{th}^{0.867} + 16.108} + 13.04 \quad (9)$$

As seen, this equation describes the relationship well for the simulated cases between the 0 and 4 m^2 K/W, and was deemed accurate. The intercept of the function is the time constant for the baseline battery pack. The function behaves asymptotically at very high thermal resistances of encapsulation.

Using Eqs. (7) and (9) in (8), the battery pack temperature, T_b, at the end of the parking phase can be computed.

$$T_b = T_\infty + (T_0 - T_\infty) \cdot exp(-t/\tau^*) \quad (10)$$

By expanding the formulation for τ^*, the equation can be rearranged to,

$$R_{th} = \left[\frac{-16.08 \left(\frac{t}{\ln\theta} + 13.04 \right)}{514.04 + \frac{t}{\ln\theta}} \right]^{\frac{1}{0.867}} \quad (11)$$

Based on this equation, a thermal resistance of 1.72 m^2 K/W is required to eliminate the need for battery heating at −20°C for a parking duration of 12 h. This value has been used in all cases with battery encapsulation in this study.

4. Vehicle simulation methodology

To capture the vehicle's performance, a transient operating cycle was used based on the recommendations from Romano et al. [31,32]. A representative cycle describing the road legal speed limit (v_{legal}), stop times, and road curvature (Y) generated as functions of distance, illustrated in Fig. 11, was chosen for this study.
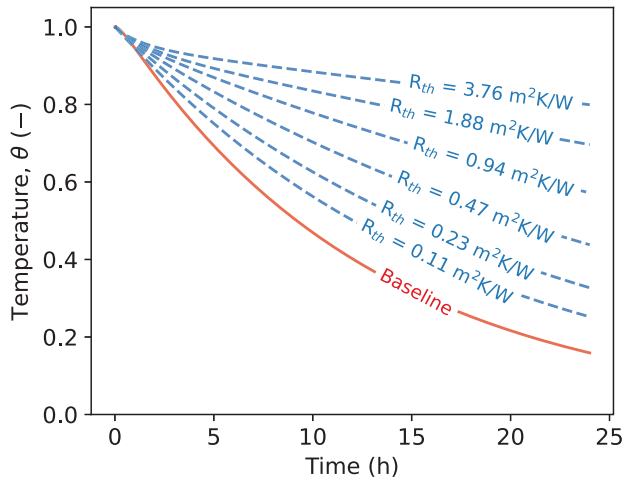
(a)
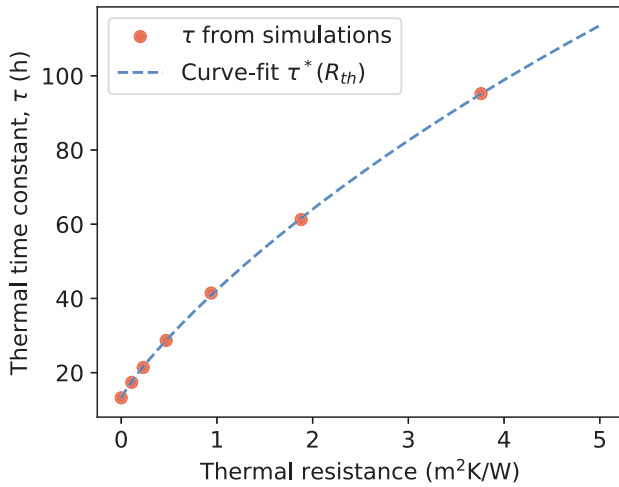
(b)

Fig. 10. (a) Variation in the battery pack temperature decay during the parking phase comparing the baseline and encapsulated configurations with increasing thermal resistance. (b) Effect of thermal resistance of encapsulation on the thermal time constant.

The driver was considered to operate such that the maximum truck speed was 25 m/s following the regulations in Sweden for heavy vehicles [33], and the lateral acceleration due to road curvature within 4.9 m/s². Thus, the target speed was defined as

$$v_{target} = \min(25, v_{legal}, \sqrt{4.9/Y}) \qquad (12)$$

Five ambient temperatures were considered, 20°C, 10°C, 0°C, −10°C, and −20°C. The simulations were performed to investigate:

1. Ambient temperature influence on the driving range and vehicle energy consumption at 70% RH and one occupant.
2. Effects of the heating load reduction strategies on the vehicle performance at 70% RH and one occupant.
3. Influence of ambient RH and number of occupants in the cabin on the effectiveness of the strategies.

A parking-driving scenario consisting of a 12 h parking period followed by driving was studied. The average battery pack temperature at the end of parking was set based on Eq. (10), with an initial
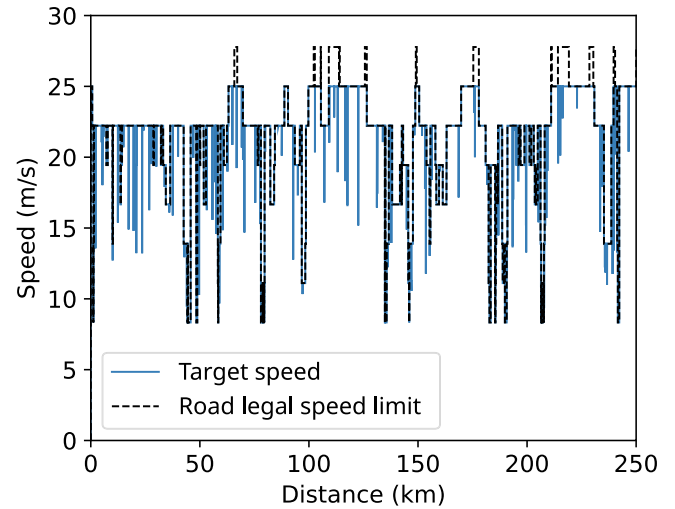

Fig. 11. Road legal speed limit and the driver's target speed as functions of distance traveled.

temperature of 23°C and the time constant corresponding to the battery pack configuration (baseline or encapsulated) for all scenarios with a parking duration of 12 h. The cabin and all cooling circuits were initialized to the same temperature as the ambient. Once the driving phase started, the driver targeted the speed obtained from the operating cycle. The battery packs were initialized to 80% SoC, and driving was carried out until it dropped to 20%. The auxiliary components were operated during the driving phase, and heating/cooling to the cabin and battery packs were provided depending on the scenarios.

For the cases with battery pack encapsulation, a thermal resistance of 1.72 m² K/W was considered as it eliminated the need for the use of battery heating at −20°C for a parking duration of 12 h, as discussed in Section 3. For the cases with cabin insulation, a thermal resistance of 4 m² K/W using a material with low thermal inertia for quicker response time was considered based on the results in [21]. The additional mass due to the cabin and battery insulation (approx. 36 kg) was included in the total mass of the truck, although it was negligible compared to the vehicle mass (20 tons).

Limitations and scope of the study

- **Battery aging effects:** In this study, the analysis is focused on the performance of the vehicle over a single cycle. The effects of cold start and battery encapsulation's effects on the cell aging are not considered.
- **Vehicle modeling:** While the vehicle, VTMS architecture and controls relevant to this study have been modeled with sufficient fidelity, several simplifications were made to reduce the computational cost such as,
  1. Modeling of the gearbox, brake compressor, and on board charger were grouped under 'Other auxiliaries' in the E-machines circuit.
  2. All components were modeled as lumped thermal masses. Though heat leakage from components and ducts were modeled through maps, the accuracy of the maps is difficult to quantify.
  3. The control strategies for E-machines, BMS, HVAC and valves are simplified as compared to that in a modern vehicle.
- **Environmental modeling:** Conditions like wind gusts, precipitation, driver behavior, topography, traffic, planned route, and so on, have not been considered in this study which can also affect
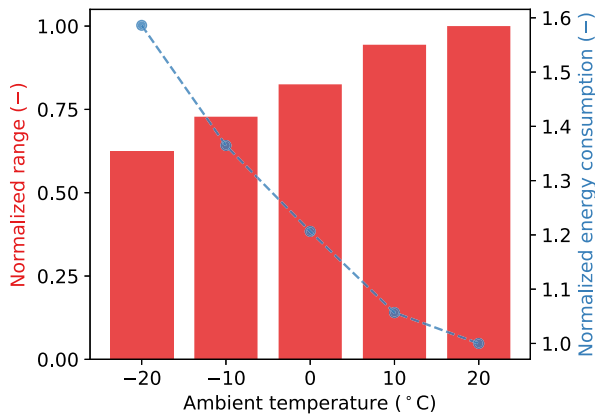
Fig. 12. Normalized range and energy consumption at different ambient temperatures for the baseline vehicle.

energy consumption and the range of the vehicle. Additionally, temperature and relative humidity were maintained constant in each simulation so that the effects can be studied systematically. However, in reality, dynamic variations of these parameters are seen.

5. Results and discussion

5.1. Ambient temperature influence on driving range and vehicle energy consumption

The ambient temperature influence on the baseline vehicle, i.e., without cabin insulation, cabin air recirculation, and battery pack encapsulation, is discussed in this subsection.

Fig. 12 describes the vehicle's range and energy consumption at the various ambient temperatures normalized to that at 20°C. The distance traveled by the vehicle decreases with decreasing ambient temperature, as much as 37.6% at −20°C. The energy consumption increases with decreasing ambient temperatures by about 58% at −20°C.

The reasons for this are explained by Fig. 13. The bars represent the degree of energy from the battery used for each influencing factor. About 8% of the energy is lost due to electrical losses for all scenarios as assumed. Most of the energy is used for traction, i.e., to overcome the aerodynamic resistance, rolling resistance, energy spent to accelerate the vehicle but lost at the friction brakes, and the losses at motors and gears, for all scenarios. However, at lower ambient temperatures, the percentage of energy used for traction decreases while the energy used for auxiliaries and battery losses (marginally) increases, which is in good agreement with the data available literature. Among the traction resistances, the contribution of the rolling resistance increases while the others decrease at low temperatures. The aerodynamic force increases at lower temperatures due to higher density. Yet, the percentage of energy in overcoming the resistance decreases due to the reduced distance traveled (see Fig. 12). Meanwhile, the rolling resistance energy usage increases even with the lower distance due to the higher rolling resistance coefficient at low temperatures. As mentioned earlier, this parameter was modeled to be temperature-dependent and increases with a decrease in tyre temperature. The mean rolling resistance coefficient of the cycle for each scenario is plotted in Fig. 14, and the values increase steadily from 0.007 at 20°C to 0.014 at −20°C.

The auxiliary energy expenditure increases by 3.5 times from 10°C to −20°C, effectively ranging from 1.98% to 7.08%, respectively. Fig. 15 illustrates the factors contributing to this increase. The mean auxiliary consumption increases fivefold, from about 1.8 kW at 10°C to 9 kW at −20°C. The main ambient temperature-dependent factors

are cabin heating, battery heating, compressor, and underhood fan. All the other auxiliaries, such as the pumps and blowers have approximately the same effect at all operating temperatures. The cabin heating load is the largest auxiliary load at low ambient temperatures as the heater operates to target a mean cabin temperature of 22°C. This is followed by battery heating for ambient temperatures below 0°C. For these scenarios, the battery pack temperature at the end of the 12 h parking phase is below the 15°C threshold as illustrated in Fig. 16, and thus battery heating is necessary. The compressor is not used at temperatures below 0°C, since dehumidification is not needed. For the duration of the cycle, the battery chiller is not used for these scenarios. Moreover, at these temperatures, the fan is employed less frequently than at 10°C and 20°C, as it was engaged only when the vehicle speed was below 10 km/h and if there was coolant flow through the radiator or refrigerant flow through the condenser.

Surprisingly, the scenario at 10°C has the lowest auxiliary energy consumption among the five scenarios as shown in Fig. 15. The main reason is that the coolant temperature in the cabin coolant circuit required to maintain the cabin at 22°C is within the same margins as the coolant temperature in the outer E-machines circuit. Thus, the valve V4 (Fig. 3) is opened, mitigating the usage of the heater in the cabin coolant circuit.

The scenario at 20°C has the second lowest auxiliary energy consumption among the considered cases. The compressor requires the most energy as it cools both the evaporator, for dehumidifying the cabin air, and the battery chiller, for cooling the battery packs. The HVAC cabin air requires cabin coolant heating to re-heat the air leaving the evaporator so that the air temperature entering the cabin is at an appropriate level.

5.2. Effects of the heating load reduction strategies on the vehicle performance

The percentage of battery energy for auxiliaries with the heating load reduction strategies and the corresponding range variation relative to the baseline are illustrated in Figs. 17(a) and 17(b). The strategies reduce the auxiliary energy consumption, consequently increasing the range for ambient temperatures below 0°C. At 10°C, encapsulating the battery increased the auxiliary energy expenditure marginally but did not have a significant effect on the range. However, using recirculation at 20°C decreases the vehicle range by about −0.6% as compared to the baseline vehicle. Additionally, when all strategies are employed together, an additive effect is seen on the vehicle range. For clarity, the effects of each strategy are discussed individually.

Cabin insulation
The objective of the insulated cabin is to reduce the ambient load (Q_{amb}), i.e., heat loss to the ambient. Fig. 18(a) presents the mean cabin inlet temperature. Analytically, at steady-state, the cabin inlet temperature (T_{in}) can be expressed as,

$$T_{in} = T_{cab} + \frac{Q_{amb}}{\dot{m}_{in}c_p} \tag{13}$$

where T_{cab} is the mean cabin temperature, $\dot{m}_{in}$ is the mass flow rate through the blower, and c_p is the specific heat of air through the heater. The heat transferred at the heater (Q_{heater}) is,

$$Q_{heater} = \dot{m}_{in}c_p(T_{in} - T_{bo}) \tag{14}$$

where T_{bo} is the temperature upstream of the heater, which is the ambient temperature in this case. The blower speed was maintained constant for each scenario. By reducing the heat loss to the ambient, the required inlet temperature is decreased and is directly responsible for reducing the energy consumption.

Due to the inlet temperature reduction, the scenarios at 0°C and 10°C are within the same margins as the coolant temperatures in the E-machines circuit, thus making it possible to use waste heat for cabin heating by opening valve V4. This is illustrated in Fig. 18(b). Thus, a slightly larger relative reduction in heating load and range saving is observed for 0°C as compared to other temperatures.
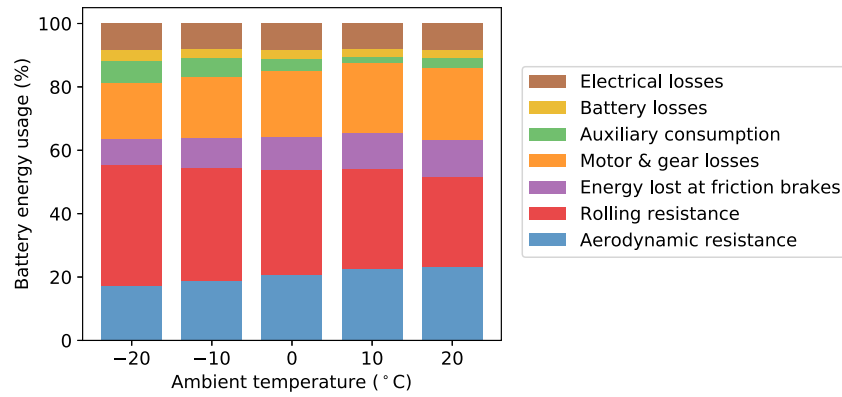
Fig. 13. Factors influencing battery energy expenditure at different ambient temperatures for the baseline vehicle.
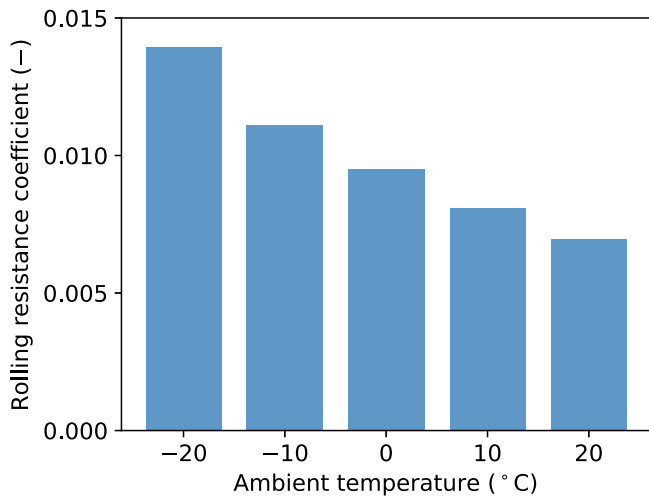

Fig. 14. Mean rolling resistance coefficient for the operating cycle at different ambient temperatures.
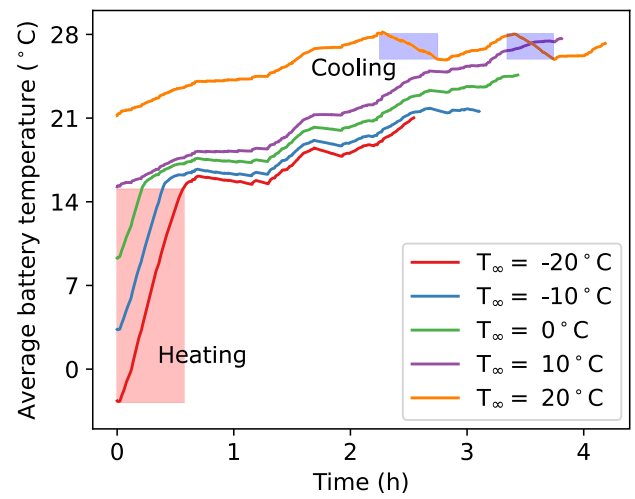

Fig. 16. Average battery pack temperature over time for several ambient temperatures. The red band represents the zone where battery heating is necessary, and the blue bands represent the regions where battery chiller is employed.
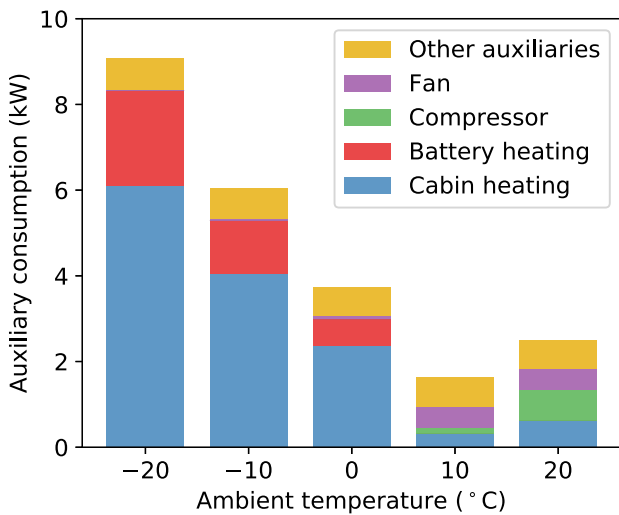

Fig. 15. Factors influencing the mean auxiliary energy consumption at different ambient temperatures.

Cabin air recirculation

By recirculating cabin air, the temperature upstream of the heater is increased thereby reducing the heating energy requirement as described in Eq. (14). The temperature upstream of the heater is given by,

$$T_{bo} = \gamma T_{cab} + (1 - \gamma)T_{\infty} \tag{15}$$

The degree of recirculation used is dependent on the target dew-point temperature. The mean front window and target dewpoint temperatures are shown in Fig. 19(a). For the current operating cycle, the mean set point margin was 11%. The target dewpoint was obtained based on Eq. (3). Thus, the RAR controller operates as shown in Fig. 19(b). From these results, the scenarios above 0°C can be classified to be CO_2-critical, with a fresh-air intake of approximately 10 g/s to maintain mean CO_2 at 1000 ppm. The scenarios at −10°C and −20°C are humidity-critical, allowing about 13.3 g/s and 21.8 g/s of fresh air, which corresponds to 84.9% and 78.5% mean return-air ratios, respectively.
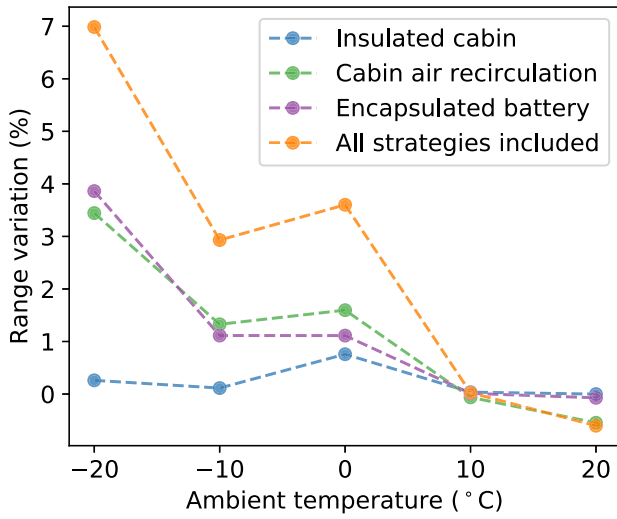
With recirculation, the mass flow rate increases through the HVAC system as shown in Fig. 19(c). The increase of about 10 g/s is due to the difference in the operating pressure in the cabin and that upstream of the blower. This lowers the inlet temperature based on Eq. (13), as shown in Fig. 18(a). Thus, valve V4 opens to allow waste heat
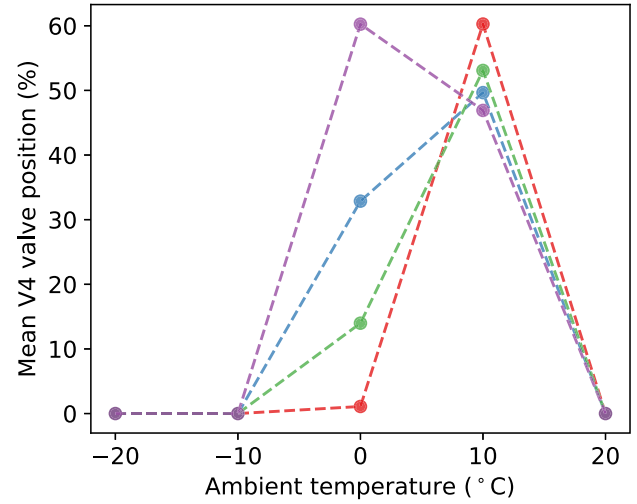
(a)
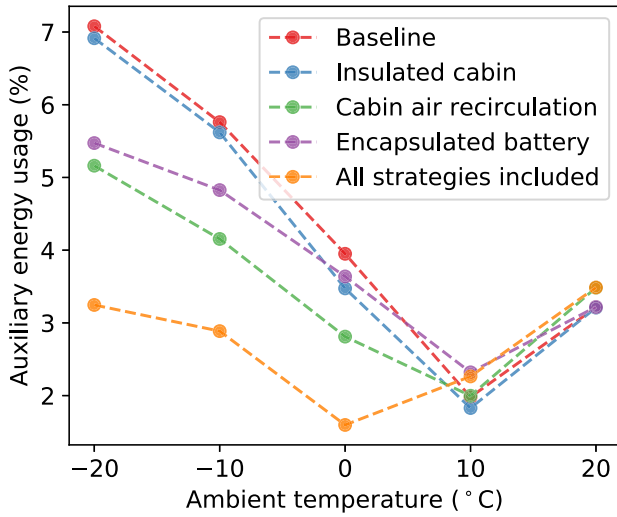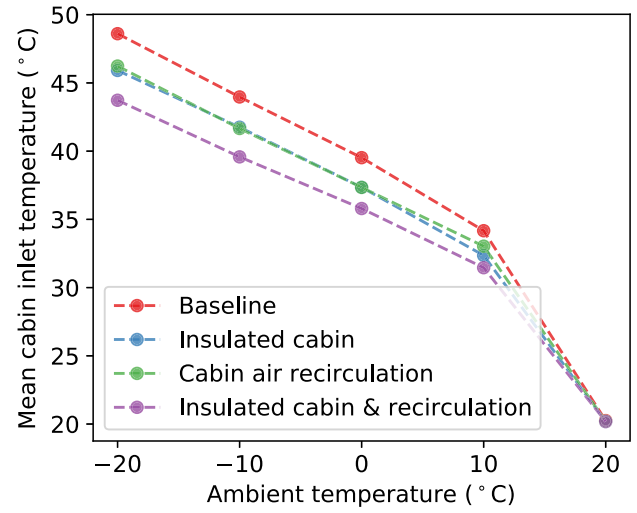
(b)

Fig. 17. Effects of heating load reduction strategies at selected ambient temperatures as compared to the baseline vehicle: (a) Percentage of battery energy used for auxiliaries, (b) Variation in vehicle range.

(a)

(b)

Fig. 18. Comparison between mean quantities from the baseline vehicle and a vehicle with insulated cabin at selected ambient temperatures: (a) Cabin inlet temperature; (b) V4 valve position (see Fig. 3).

from the E-machines circuit to be used for cabin heating, Fig. 18(b). However, due to the higher mass flow rate with recirculation, more energy is extracted through the heater, which means that the coolant temperature on the outer loop (E-machines circuit) decreases. Thus, valve V4 closes more often than with cabin insulation.

Another consequence of using cabin air recirculation at 10°C, and 20°C is that the evaporator heat transfer varies as shown in Fig. 20(a). At these temperatures, the cabin air at 22°C mixes with the colder ambient air, effectively increasing the air temperature upstream of the evaporator. This increases the energy required to cool down the air to 3°C at the evaporator and is the reason for the increased energy consumption at 10°C as shown in Fig. 20(b). However, at 20°C, a small decrease in evaporator heat transfer is noted despite the above argument. The reason for this is that the ambient air has 70% RH while the cabin air has about 30%. At the evaporator, condensation is exothermic and so, the compressor must work against this effect. Since the cabin air is less humid than the ambient air, the energy required

while recirculating air is lower. However, the cabin heating load at 20°C increases with recirculation as shown in Fig. 21, due to higher mass flow rate with recirculation as explained earlier. This is believed to be the main reason for the slight decrease in vehicle range at 20°C seen in Fig. 17(b). Thus, it is recommended to adjust fan operation when recirculation is employed at 20°C, and to refrain from using recirculation when dehumidification is necessary, and if the ambient temperature is below 20°C.

The outcome of these effects is that the cabin heating load reduces for temperatures below 10°C, see Fig. 21. The heating load reduction with the cabin air recirculation is much greater than with the insulated cabin, suggesting that the ventilation load reduction is more effective than ambient load reduction, which is in line with the discussions in [7,18,34]. As seen before, combining the two strategies results in an additive effect.

Battery pack encapsulation

As discussed in Section 3, by insulating the battery pack, its temperature can be retained at a sufficiently high value so that the energy
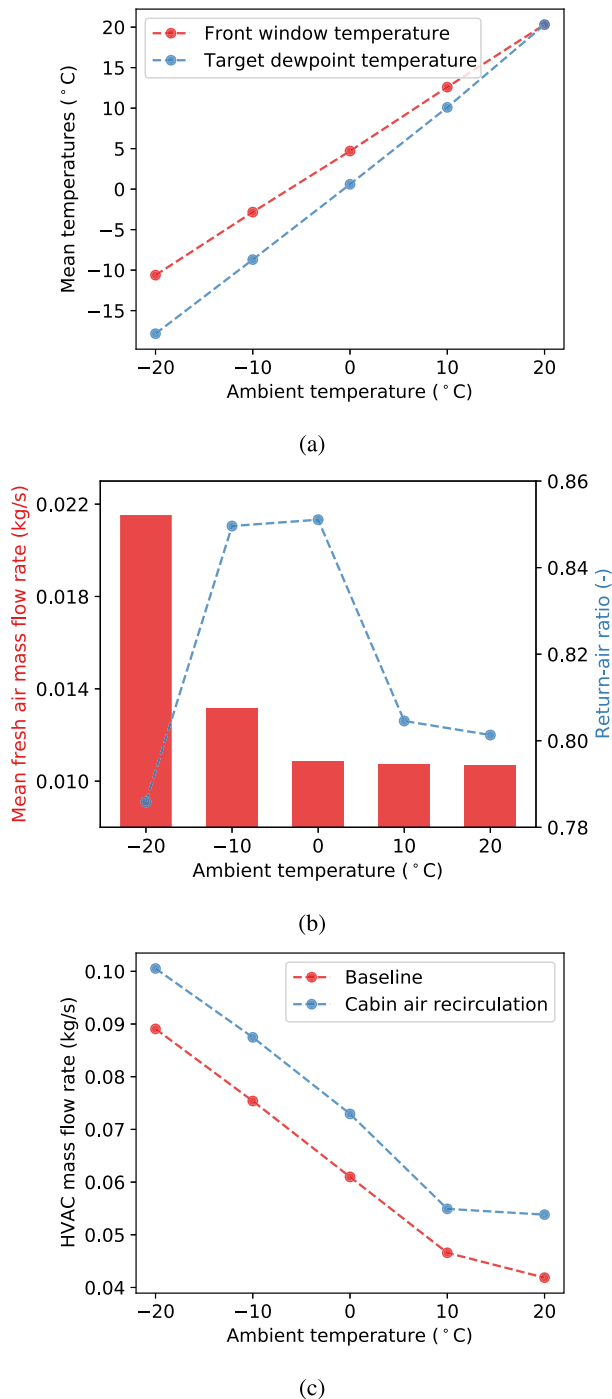
(a)

(b)

(c)

Fig. 19. (a) Front window and target dew-point temperatures; (b) Fresh air mass flow rate and return-air ratio (c) Comparison of the HVAC mass flow rate between the baseline vehicle and with cabin air recirculation.

(a)

(b)

Fig. 20. Comparison between mean quantities from the baseline vehicle and a vehicle with cabin air recirculation at selected ambient temperatures: (a) Evaporator heat transfer rate; (b) Compressor power.

required for battery heating in the subsequent cycles after parking for a long time can be mitigated. The thermal resistance of 1.72 m^2 K/W used for encapsulation, eliminated the need for battery heating when the parking duration was 12 h even at −20°C. Meanwhile, due to high insulation, the cooling requirement of the battery packs increases slightly. The battery packs are now entirely reliant on the cooling system, which increases the demand on the refrigerant system. The insulated battery pack temperatures are plotted in Fig. 22(a), and it can be seen that temperatures reach the threshold for chiller employment at a faster rate than the baseline packs, shown in Fig. 16. The energy
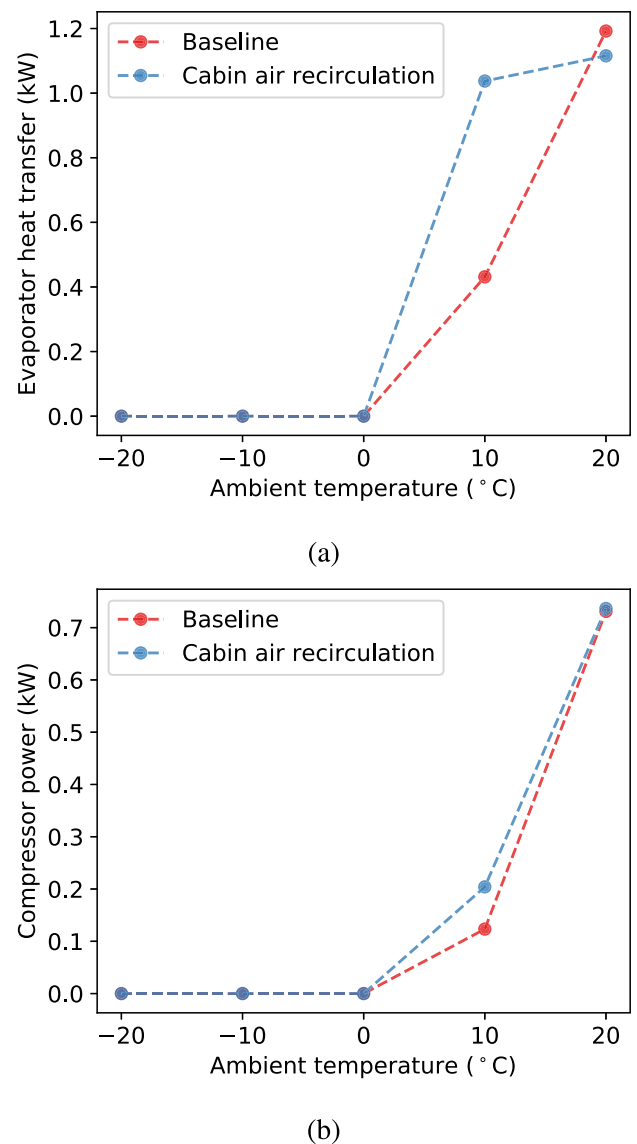
spent cooling the insulated battery pack is greater than the baseline pack for ambient temperatures above −10°C as shown in Fig. 22(b). Nevertheless, the energy gain from using battery pack encapsulation for cases below 0°C outweighs the energy expenditure due to chiller employment during one battery cycle as seen earlier in Fig. 17.

5.3. Influence of ambient RH and number of occupants in the cabin on the effectiveness of the strategies

Among the strategies investigated in this study, cabin air recirculation is sensitive to two other parameters namely, the ambient humidity, and the number of occupants in the cabin. The two parameters were varied and results for the same cycle are presented in this subsection. The heat, humidity, CO_2, and mass of the second occupant were included appropriately. A parametric study of 70% and 90% RH, and one and two occupants were evaluated on the vehicle configurations with all the strategies.

Fig. 23(a) compares the cabin heating load of the vehicle with all strategies among the scenarios with varying number of occupants and
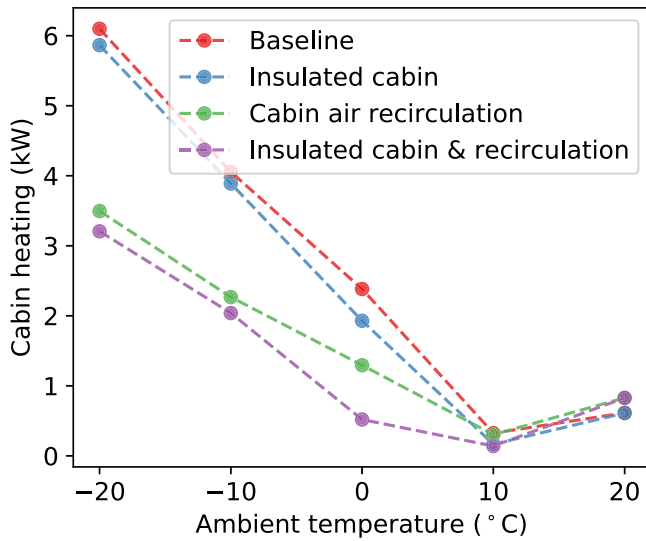
Fig. 21. Comparison between mean cabin heating load for the baseline vehicle, and configurations with insulated cabin, cabin air recirculation, and combined cabin insulation and cabin air recirculation.

RH. At −10°C and −20°C, the heating load slightly increases when two occupants are present, and at 90% RH as compared to one occupant and 70% RH. The main reason is because of fresh air flow rate (Fig. 23(b)) and return-air ratios (Fig. 23(c)) employed to prevent fogging and to maintain a 1000 ppm CO_2 concentration. When two occupants are present in the cabin, the vapor and CO_2 sources in the cabin increase and hence, more fresh air is needed to satisfy the constraints. When operating at 90% ambient RH, more fresh air is needed to prevent fogging. The employed RAR reduces at 0°C, indicating that the condition is humidity critical. For ambient temperatures above 0°C, the cabin heating load with two occupants is lower than that with one occupant. This is because of the increased metabolic heat load with the additional occupant, effectively reducing the HVAC energy required to maintain 22°C in the cabin.

The consequence of the higher heating load at sub-zero temperatures is that the increase in range experienced with the investigated strategies at low temperatures decreases. Fig. 24 presents the range variation among the four cases relative to the baseline vehicle with one occupant and 70% ambient RH. At −10°C and −20°C, since the energy for cabin heating is predominantly from the heater in the cabin coolant circuit, decreasing the return-air ratio reduces the range gains. At 0°C, however, a significant portion of the energy is derived from waste heat and therefore, this effect is mitigated. Above 10°C, no significant range variations are noted.

6. Conclusion

The transition to battery electric vehicles has introduced several challenges for vehicle thermal management systems, especially in ensuring proper climate control for the passenger cabin, battery pack, and motors, all while maintaining driving range. Environmental factors, particularly low ambient temperatures, are known to significantly affect vehicle energy consumption. For this reason, this study focuses on energy-saving strategies for BEVs in cold climates, aiming to reduce heating consumption at the component level. The current study utilized vehicle simulations of an electric truck to evaluate energy consumption under parking and driving scenarios. A complete vehicle simulation framework was developed, incorporating various subsystems. The cabin and battery pack models were validated against calibrated high-fidelity models and measurement data. A strategy was developed to determine the target dew-point temperature for cabin air recirculation under
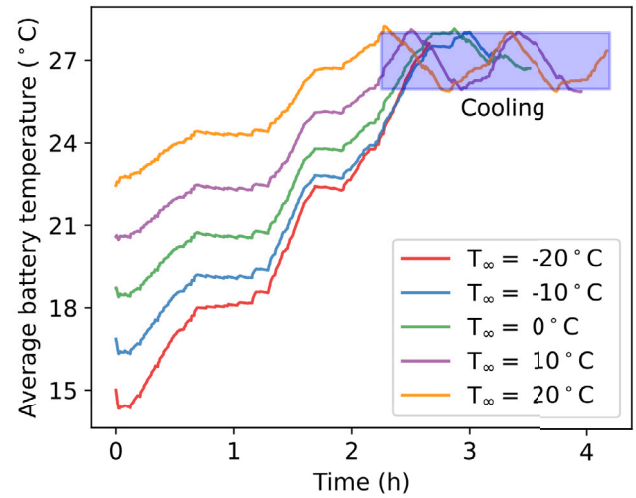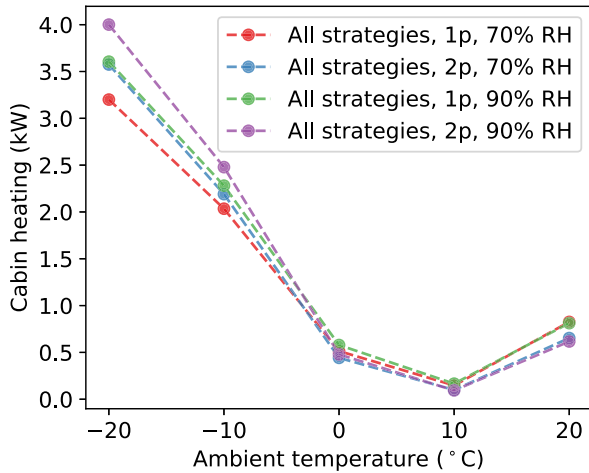

(a)
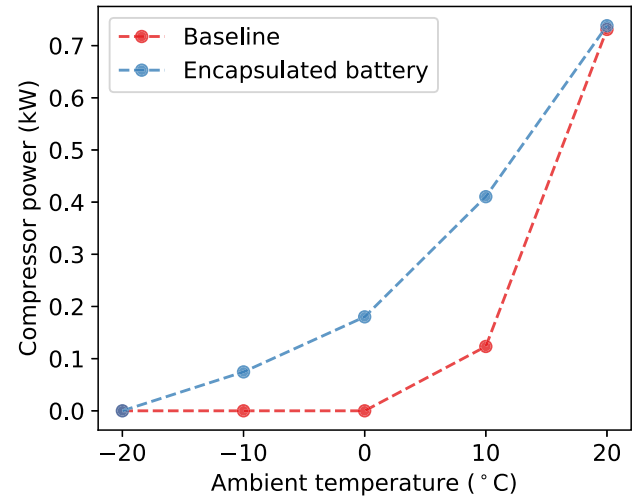
(b)

Fig. 22. Battery pack encapsulation analysis: (a) Average battery pack temperature; (b) Comparison of compressor power between the baseline and pack-encapsulated vehicles at selected ambient temperatures.
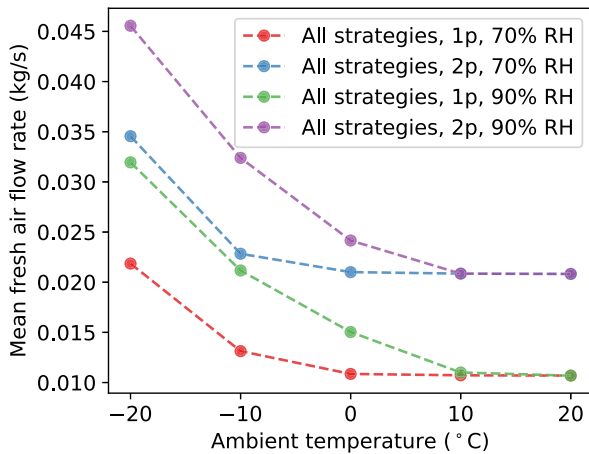
dynamic conditions, and an empirical formula was derived to calculate the thermal resistance needed to maintain battery pack temperatures above heating thresholds during long parking periods.

Heating load reduction strategies for the cabin and battery pack, namely, cabin insulation, cabin air recirculation, and battery pack encapsulation, were investigated for five ambient temperature, two relative humidity levels, and varying number of occupants. The key conclusions of the study are as follows:
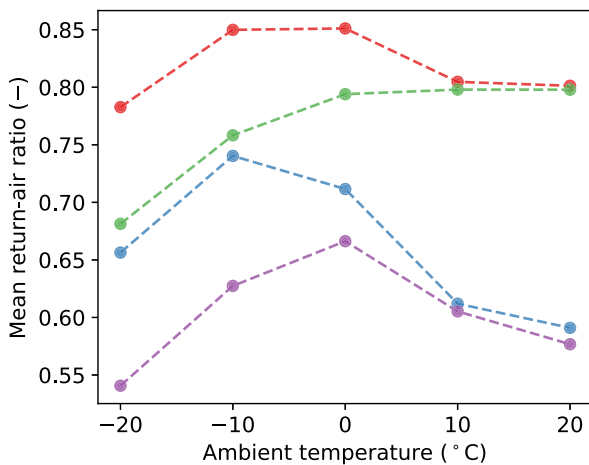
1. During the driving phase of the baseline vehicle, the auxiliary energy usage relative to the available battery energy increased by 5.1% from 10°C to −20°C. The cabin heating load was the largest load below 0°C, followed by battery heating.

2. With cabin insulation, the heat losses from cabin air to the ambient were reduced, which resulted in a decrease in the cabin inlet temperature to maintain the cabin at 22°C. With cabin air recirculation, the ventilation load was reduced by increasing the upstream temperature of the heater for conditions below 0°C. An additive effect was noted when both strategies were combined.

Fig. 24. Variation in vehicle range with heating load reduction strategies illustrating the effect of ambient RH, and number of cabin occupants, relative to the baseline vehicle at selected temperatures.

3. With battery pack thermal encapsulation of 1.72 m^2 K/W, the battery heating load was eliminated for all cases, but increased the battery chiller engagement for scenarios above −10°C. Nevertheless, the range improved with battery pack encapsulation for ambient temperatures below 0°C.

4. The combined effects of all strategies had a cumulative effect. The vehicle range increases for low ambient temperatures, and up to about 7% at −20°C while operating at 70% RH and one occupant. At higher RH and more occupants, the range gains were somewhat reduced.

Fig. 23. Analysis of ambient RH and number of occupants in the cabin on the vehicle with all strategies at selected temperatures: (a) Mean cabin heating load; (b) Mean fresh air flow rate; (c) Mean return-air ratio.
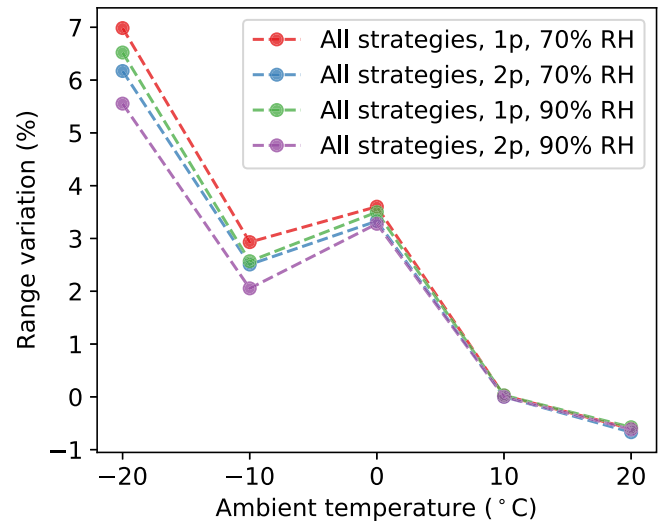
CRediT authorship contribution statement

Anandh Ramesh Babu: Writing – original draft, Visualization, Validation, Methodology, Investigation, Formal analysis, Data curation, Conceptualization. **Simone Sebben:** Writing – review & editing, Supervision, Software, Resources, Project administration, Funding acquisition, Conceptualization. **Zenitha Chronéer:** Writing – review & editing, Supervision, Project administration, Investigation, Conceptualization. **Sassan Etemad:** Writing – review & editing, Supervision, Software, Resources, Project administration, Investigation, Conceptualization.

Declaration of competing interest

The authors declare that they have no known competing financial interests or personal relationships that could have appeared to influence the work reported in this paper.

Data availability

The authors do not have permission to share data.

References

[1] John Taggart, Ambient temperature impacts on real-world electric vehicle efficiency & range, in: 2017 IEEE Transportation Electrification Conference and Expo, ITEC, 2017, pp. 186–190, http://dx.doi.org/10.1109/ITEC.2017.7993269.

[2] Jukka Hyttinen, Matthias Ussner, Rickard Österlöf, Jenny Jerrelind, Lars Drugge, Truck tyre transient rolling resistance and temperature at varying vehicle velocities - Measurements and simulations, Polym. Test. (ISSN: 0142-9418) 122 (2023) 108004, http://dx.doi.org/10.1016/j.polymertesting.2023.108004, URL https://www.sciencedirect.com/science/article/pii/S0142941823000843.

[3] Yazan Al-Wreikat, Clara Serrano, José Ricardo Sodré, Effects of ambient temperature and trip characteristics on the energy consumption of an electric vehicle, Energy (ISSN: 0360-5442) 238 (2022) 122028, http://dx.doi.org/10.1016/j.energy.2021.122028, URL https://www.sciencedirect.com/science/article/pii/S0360544221022763.

[4] Tugce Yuksel, Jeremy J. Michalek, Effects of regional temperature on electric vehicle efficiency, range, and emissions in the United States, Environ. Sci. Technol. (ISSN: 0013-936X) 49 (6) (2015) 3974–3980, URL https://doi.org/10.1021/es505621s.

[5] Matthias Steinstraeter, Tobias Heinrich, Markus Lienkamp, Effect of low temperature on electric vehicle range, World Electr. Veh. J. (ISSN: 2032-6653) 12 (3) (2021) 115, http://dx.doi.org/10.3390/wevj12030115, URL https://www.mdpi.com/2032-6653/12/3/115.

[6] Filip Nielsen, Åsa Uddheim, Jan-Olof Dalenbäck, Potential energy consumption reduction of automotive climate control systems, Appl. Therm. Eng. (ISSN: 1359-4311) 106 (2016) 381–389, http://dx.doi.org/10.1016/j.applthermaleng.2016.05.137, URL https://www.sciencedirect.com/science/article/pii/S1359431116308158.

[7] Ziqi Zhang, Wanyong Li, Chengquan Zhang, Jiangping Chen, Climate control loads prediction of electric vehicles, Appl. Therm. Eng. (ISSN: 1359-4311) 110 (2017) 1183–1188, http://dx.doi.org/10.1016/j.applthermaleng.2016.08.186, URL https://www.sciencedirect.com/science/article/pii/S1359431116315459.

[8] Ganesan Nagasubramanian, Electrical characteristics of 18650 Li-ion cells at low temperatures, J. Appl. Electrochem. (ISSN: 1572-8838) 31 (1) (2001) 99–104, URL https://doi.org/10.1023/A:1004113825283.

[9] Yan Ji, Yancheng Zhang, Chao-Yang Wang, Li-ion cell operation at low temperatures, J. Electrochem. Soc. (ISSN: 1945-7111) 160 (4) (2013) A636, http://dx.doi.org/10.1149/2.047304jes, URL https://iopscience.iop.org/article/10.1149/2.047304jes/meta.

[10] S.S. Zhang, K. Xu, T.R. Jow, The low temperature performance of Li-ion batteries, J. Power Sources (ISSN: 0378-7753) 115 (1) (2003) 137–140, http://dx.doi.org/10.1016/S0378-7753(02)00618-3, URL https://www.sciencedirect.com/science/article/pii/S0378775302006183.

[11] Thomas Waldmann, Marcel Wilka, Michael Kasper, Meike Fleischhammer, Margret Wohlfahrt-Mehrens, Temperature dependent ageing mechanisms in Lithium-ion batteries – A Post-Mortem study, J. Power Sources (ISSN: 0378-7753) 262 (2014) 129–135, http://dx.doi.org/10.1016/j.jpowsour.2014.03.112, URL https://www.sciencedirect.com/science/article/pii/S0378775314004352.

[12] Jiang Fan, Steven Tan, Studies on charging Lithium-ion cells at low temperatures, J. Electrochem. Soc. (ISSN: 1945-7111) 153 (6) (2006) A1081, http://dx.doi.org/10.1149/1.2190029, URL https://iopscience.iop.org/article/10.1149/1.2190029/meta.

[13] Gabriele Leoncini, Ronan Mothier, Benoît Michel, Marc Clausse, A review on challenges concerning thermal management system design for medium duty electric vehicles, Appl. Therm. Eng. (ISSN: 1359-4311) 236 (2024) 121464, http://dx.doi.org/10.1016/j.applthermaleng.2023.121464, URL https://www.sciencedirect.com/science/article/pii/S135943112301493X.

[14] Jae Hwan Ahn, Hoon Kang, Ho Seong Lee, Hae Won Jung, Changhyun Baek, Yongchan Kim, Heating performance characteristics of a dual source heat pump using air and waste heat in electric vehicles, Appl. Energy (ISSN: 0306-2619) 119 (2014) 1–9, http://dx.doi.org/10.1016/j.apenergy.2013.12.065, URL https://www.sciencedirect.com/science/article/pii/S0306261914000051.

[15] Tianyang Yang, Huiming Zou, Mingsheng Tang, Changqing Tian, Yuying Yan, Experimental performance of a vapor-injection CO2 heat pump system for electric vehicles in -30 °C to 50 °C range, Appl. Therm. Eng. (ISSN: 1359-4311) 217 (2022) 119149, http://dx.doi.org/10.1016/j.applthermaleng.2022.119149, URL https://www.sciencedirect.com/science/article/pii/S1359431122010808.

[16] Guiying Zhang, Huiming Zou, Fei Qin, Qingfeng Xue, Changqing Tian, Investigation on an improved heat pump AC system with the view of return air utilization and anti-fogging for electric vehicles, Appl. Therm. Eng. (ISSN: 1359-4311) 115 (2017) 726–735, http://dx.doi.org/10.1016/j.applthermaleng.2016.12.143, URL https://www.sciencedirect.com/science/article/pii/S1359431116345070.

[17] Miyoko Oiwake, Ozeki Yoshiichi, Sogo Obata, Hideaki Nagano, Itsuhei Kohri, Effects of the glass and body heat transfer characteristics of a hybrid electric vehicle on its fuel consumption and cruising distance, in: WCX™ 17: SAE World Congress Experience, 2017, pp. 2017–01–0184, http://dx.doi.org/10.4271/2017-01-0184, URL https://www.sae.org/content/2017-01-0184/.

[18] Matthew A. Jeffers, Larry Chaney, John P. Rugh, Climate control load reduction strategies for electric drive vehicles in cold weather, SAE Int. J. Passeng. Cars - Mech. Syst. (ISSN: 1946-4002) 9 (1) (2016) 75–82, http://dx.doi.org/10.4271/2016-01-0262, URL https://www.sae.org/content/2016-01-0262/.

[19] Leila Ghadbeigi, Brandon Day, Kristina Lundgren, Taylor D. Sparks, Cold temperature performance of phase change material based battery thermal management systems, Energy Rep. (ISSN: 2352-4847) 4 (2018) 303–307, http://dx.doi.org/10.1016/j.egyr.2018.04.001, URL https://www.sciencedirect.com/science/article/pii/S2352484718300428.

[20] Shinichiro Hirai, Takuya Kataoka, Tatsumi Kumada, Takaaki Goto, The humidity control system applied to reduce ventilation heat loss of HVAC systems, in: SAE 2011 World Congress & Exhibition, 2011, http://dx.doi.org/10.4271/2011-01-0134, URL https://www.sae.org/content/2011-01-0134/.

[21] Anandh Ramesh Babu, Simone Sebben, Tore Bark, Effect of cabin insulation on the heating performance in EVs at low temperatures, in: SAE WCX Conference, SAE Technical Papers, Detroit, Michigan, United States, 2023, http://dx.doi.org/10.4271/2023-01-0763, URL https://www.sae.org/content/2023-01-0763.

[22] Anandh Ramesh Babu, Simone Sebben, Zenitha Chronéer, Sassan Etemad, An adaptive cabin air recirculation strategy for an electric truck using a coupled CFD-thermoregulation approach, Int. J. Heat Mass Transfer (ISSN: 0017-9310) 221 (2024) 125056, http://dx.doi.org/10.1016/j.ijheatmasstransfer.2023.125056, URL https://www.sciencedirect.com/science/article/pii/S0017931023012012.

[23] Anandh Ramesh Babu, Blago Minovski, Simone Sebben, Thermal encapsulation of large battery packs for electric vehicles operating in cold climate, Appl. Therm. Eng. (ISSN: 1359-4311) 212 (2022) 118548, http://dx.doi.org/10.1016/j.applthermaleng.2022.118548, URL https://www.sciencedirect.com/science/article/pii/S1359431122004999.

[24] Wolf-Heinrich Hucho, Aerodynamics of Road Vehicles, fourth ed., Vol. 4, SAE International, New York, ISBN: 0-7680-0029-7, 1998.

[25] Anandh Ramesh Babu, Jelena Andric, Blago Minovski, Simone Sebben, System-level modeling and thermal simulations of large battery packs for electric trucks, Energies (ISSN: 1996-1073) 14 (16) (2021) 4796, http://dx.doi.org/10.3390/en14164796, URL https://www.mdpi.com/1996-1073/14/16/4796.

[26] Tarun Huria, Massimo Ceraolo, Javier Gazzarri, Robyn Jackey, High fidelity electrical model with thermal dependence for characterization and simulation of high power lithium battery cells, in: 2012 IEEE International Electric Vehicle Conference, 2012, pp. 1–8, http://dx.doi.org/10.1109/IEVC.2012.6183271, URL https://ieeexplore.ieee.org/document/6183271.

[27] Dawn Bernardi, Ellen Pawlikowski, John Newman, A general energy balance for battery systems, J. Electrochem. Soc. (ISSN: 1945-7111) 132 (1) (1985) 5, http://dx.doi.org/10.1149/1.2113792, URL https://iopscience.iop.org/article/10.1149/1.2113792/meta.

[28] Dixin Wei, Filip Nielsen, Hannes Karlsson, Lars Ekberg, Jan-Olof Dalenbäck, Vehicle cabin air quality: Influence of air recirculation on energy use, particles, and CO2, Environ. Sci. Pollut. Res. (ISSN: 1614-7499) 30 (15) (2023) 43387–43402, URL https://doi.org/10.1007/s11356-023-25219-x.

[29] Tong-Bou Chang, Jer-Jia Sheu, Jhong-Wei Huang, Yu-Sheng Lin, Che-Cheng Chang, Development of a CFD model for simulating vehicle cabin indoor air quality, Transp. Res. Part D: Transp. Environ. (ISSN: 13619209) 62 (2018) 433–440, http://dx.doi.org/10.1016/j.trd.2018.03.018, URL https://linkinghub.elsevier.com/retrieve/pii/S1361920917309744.

[30] Frank P. Incropera, Fundamentals of Heat and Mass Transfer, Sixth ed., Vol. 6, Wiley, New York, ISBN: 978-0-471-45728-2, 2013.

[31] Luigi Romano, Michele Godio, Pär Johannesson, Fredrik Bruzelius, Toheed Ghandriz, Bengt Jacobson, Development of the västra götaland operating cycle for long-haul heavy-duty vehicles, IEEE Access (ISSN: 2169-3536) 11 (2023) 73268–73302, http://dx.doi.org/10.1109/ACCESS.2023.3295989, URL https://ieeexplore.ieee.org/document/10184427/.

[32] Luigi Romano, The Operating Cycle Representation of Road Transport Missions (Ph.D. thesis), Chalmers University of Technology, Sweden, ISBN: 9789179058883, 2023, URL https://research.chalmers.se/en/publication/536236.

[33] Road Rules and Safety in Sweden. URL https://europa.eu/youreurope/citizens/travel/driving-abroad/road-rules-and-safety/sweden/index_en.htm.

[34] Ziqi Zhang, Dandong Wang, Chengquan Zhang, Jiangping Chen, Electric vehicle range extension strategies based on improved AC system in cold climate – A review, Int. J. Refrig. (ISSN: 0140-7007) 88 (2018) 141–150, http://dx.doi.org/10.1016/j.ijrefrig.2017.12.018, URL https://www.sciencedirect.com/science/article/pii/S0140700718300033.